

Mass Transfer of Ozone Using a Microporous Diffuser Reactor System

Marie M. Mitani,¹ Arturo A. Keller,¹ Orville C. Sandall,² and Robert G. Rinker²

¹Bren School of Environmental Science & Management, University of California, Santa Barbara, CA, USA

²Department of Chemical Engineering, University of California, Santa Barbara, CA, USA

An ozone reactor was constructed using a tubular gas diffuser made of microporous stainless steel to significantly reduce gas bubble size and increase overall mass transfer area. Overall mass transfer coefficient, K_{La} [s^{-1}], was correlated with gas (G) and liquid (L) flow rates using $K_{La} = AL^\alpha G^\beta$, with $A = 3.96 \times 10^8$ [s^{-1}], $\alpha = 1.53$, and $\beta = 0.40$, with L and G in [$m^3 s^{-1}$]. The reactor is essentially plug flow at high G or L . This system achieves one of the highest ozone mass transfer rates observed in the literature.

Keywords Ozone, Reactor Design, Contactor Design, Microporous Diffuser, Water Treatment, Remediation, Mass Transfer Coefficient

INTRODUCTION

Ozone treatment of wastewater and drinking water has been used for decades and is a well-known technology. In some cases, ozone treatment alone adequately degrades contaminants to meet water quality standards (Rinker et al., 1999). Ozone can also be combined with hydrogen peroxide dissolved in the aqueous stream to produce high oxidation rates. Current treatment systems using ozone have been limited due to the high cost of operation as well as by-product concerns. A common problem associated with ozone oxidation of aqueous contaminants is the low rate of mass transfer of ozone to the aqueous phase and the loss of ozone to the overlying headspace. Most systems compensate for these limitations by increasing the amount of ozone used, resulting in expensive initial capital as well as operating and maintenance costs.

Address correspondence to Arturo A. Keller, University of California at Santa Barbara, Bren School of Environmental Science, Santa Barbara, California 93106. E-mail: keller@bren.ucsb.edu

Ozone mass transfer rate is, in most cases, the limiting step in the destruction of pollutants in water treatment. If this rate were greatly increased by an appropriate reactor design, then costs associated with water treatment could be effectively reduced. Therefore, the method of gas-liquid contacting is a critical aspect of the ozonation process.

It has been found that even with gas bubbles having diameters as low as 1 mm, the ozone mass transfer rate remains limiting and ozone is lost in the headspace (Le Sauze et al., 1993). Since interfacial area drives the mass transfer process, bubble size and degree of coalescence are crucial in determining the rate of mass transfer and the oxidative potential of ozone in the system. Mass transfer rates of gas to liquid for varying bubble sizes have been calculated using computer simulations and also measured experimentally for different systems (Boufaif and Roustan, 1998; Mtarjemi and Jameson, 1978; Ohkawa et al., 1983). As expected, these studies showed that the smaller the bubble size, the greater the mass transfer rate of gas. The larger surface area to volume ratio of very small bubbles provides an overall larger area for ozone mass transfer to occur. A study of the mass transfer from very small oxygen bubbles in tap water showed that the best oxygen transfer rate came from bubbles less than 1 mm in diameter in the range of 300–1000 μm (Qiu et al., 2001).

The reactor used for this study includes a porous diffuser that produces sub-micron bubbles. The diffuser extends concentrically throughout the length of the cylindrical reactor in order to increase the contact time between dissolved ozone and pollutants as well as to increase the interfacial area between the gas and liquid. Though coalescence occurs in the top portion of the reactor, fine bubbles appear throughout the length of the reactor, thus creating a very large surface area to optimize the mass transfer rate of ozone. The purpose of this study was to show how a microporous diffuser system, as well as the reactor configuration, could optimize an ozone oxidation system. Since the success

of a water treatment method using ozone is in most cases dependent on the rate of mass transfer, a reactor system that could improve this rate can make this option cost effective and feasible to use. A literature search did not reveal that a reactor of this type has previously been tested for ozone mass transfer from gas to liquid prior to this study.

To provide a comparison of the performance of this reactor to others in the field, the mass transfer coefficient, $K_L a [s^{-1}]$, must first be determined, where K_L = the overall mass transfer coefficient based on a liquid phase driving force [ms^{-1}] and a = interfacial area for mass transfer per unit volume [m^{-1}]. A comparison of $K_L a$ for ozone under similar experimental conditions, such as temperature and pressure, can determine the performance of the reactor in relation to others in the field. $K_L a$ ranged from 0.0083 to 0.025 s^{-1} for bubble reactors (Roustan et al., 1996; Zhou and Smith, 2000).

In order to model the reactor system, it was necessary to define the reactor configuration. The reactor had two main sections, the annular area of the diffuser and the mixing area above the diffuser (Figure 1). Although the reactor should behave nearly as plug flow, to model the reactor more accurately the residence time distribution (RTD) of the reactor was determined using an inorganic tracer. Since the reactor was contained in glass tubing, it was also possible to make a qualitative assessment of mixing conditions by observing a pulse of dye as it flowed through the reactor.

The steady state species balance, considering axial dispersion, is given by:

$$-u_L \left(\frac{dC_{OL}}{dz} \right) + D_i \left(\frac{d^2 C_{OL}}{dz^2} \right) + K_L a (C_{OL}^* - C_{OL}) = 0 \quad [1]$$

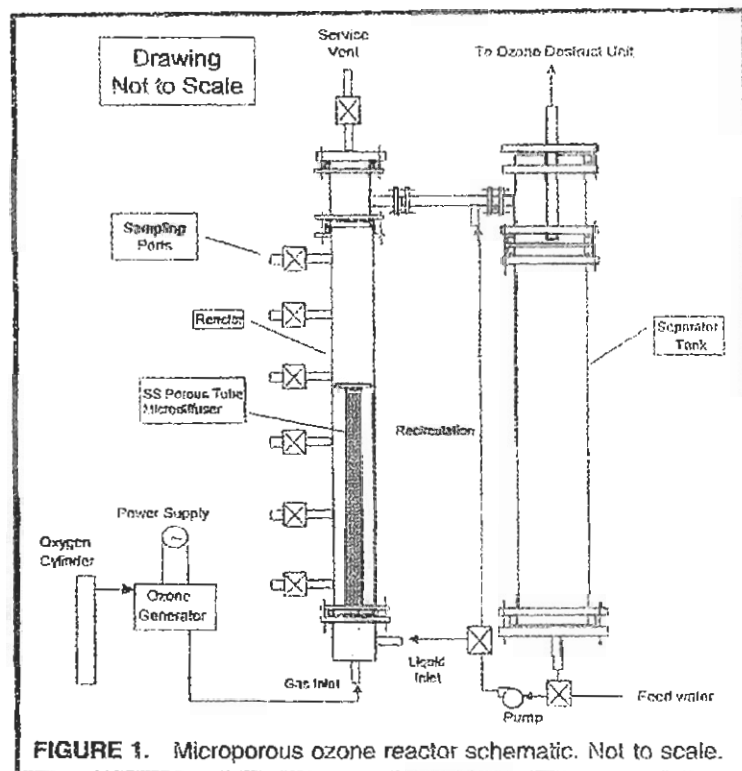


FIGURE 1. Microporous ozone reactor schematic. Not to scale.

where u_L = liquid velocity [ms^{-1}], z = vertical coordinate [m], C_{OL} = molar concentration of ozone in the aqueous phase [$mol m^{-3}$], C_{OL}^* = molar concentration of ozone in the aqueous phase in equilibrium with the gas phase at the gas/liquid interface [$mol m^{-3}$], D_i = axial dispersion coefficient [$m^2 s^{-1}$]. Introducing the second-order transport term allows the model to predict the reactor performance more precisely. The value of D_i can be determined experimentally by measuring the RTD. This allows us to fully characterize the reactor for scale-up.

EXPERIMENTAL METHODS

All mass transfer experiments were conducted in a cylindrical reactor consisting of a 0.025 m diameter glass tube with a height of 1.24 m. A 0.0125 m diameter Mott porous stainless steel tube (Mott Corporation, Farmington, CT, USA), 0.914 m in length, with average pore size of 0.5 μm , was concentrically located inside the glass tube. Water flowed axially in the annulus between the diffuser and the glass wall. Six sample ports were installed along the length of the reactor. The reactor was mounted vertically to achieve uniform and axially co-current bubble flow (Figure 1). These experiments were conducted without recirculation.

Water flow rates ranged from 3.33×10^{-6} to $2.08 \times 10^{-5} m^3 s^{-1}$, for each corresponding gas flow rate. Deionized water with pH 6 was used. The gas flow rate ranged from 1.45×10^{-6} to $1.67 \times 10^{-5} m^3 s^{-1}$, with the pressure exiting the ozone generator set at 20 psi. Ozone was produced by an Ozonia CFS-2A Ozone Generator (Ozonia North America, Elmwood Park, NJ, USA). Ozone gas concentrations were determined using an IN USA H-1 Ozone Gas Analyzer (IN USA Corp., Needham, MA, USA). Aliquot liquid samples of 2.0 mL were withdrawn from the ports along the reactor and pipetted into 0.10 mL of indigo reagent. Ozone concentrations in the aqueous phase were measured using the standard indigo dye method (Bader and Hoigne, 1982). Typical gas concentrations of ozone in oxygen ranged from 78 to 81 g/m^3 . The steady-state reactor temperature was maintained at ~ 296 K. All experiments for the measurement of ozone concentrations were run in duplicates with a reproducibility of $\pm 2.5\%$.

Residence Time Distribution (RTD)

The RTD was measured by introducing 5 mL of a salt solution, 1.0 M KNO_3 , as an impulse into the inlet stream of the reactor and measuring the time dependent conductivity of the liquid leaving the reactor at gas and liquid flow rates that corresponded to the ozone mass transfer experiments. The gas used for these experiments was oxygen, with no ozone. Water samples were collected at the sample port at the end of the diffuser. The conductivity was measured using a Fisher Scientific Digital Conductivity Meter with an insertion probe. Samples were collected in 20 mL or 40 mL

vials in timed increments ranging from 1.68 to 13.7 seconds in order to obtain the conductivity profile, which is a graphic measure of the dispersion characteristics in the reactor. Conductivity experiments were run in triplicates with a reproducibility of $\pm 10\%$.

To determine the dimensionless dispersion number, D_L [-], where $D_L = \frac{D_i}{u_L l}$, and l = length [m], we used the definition of the variance, σ^2 , given by (10):

$$\sigma^2 = \frac{\sum t_i^2 C_i}{\sum C_i} - t_E^2 = \frac{\sum t_i^2 C_i}{\sum C_i} - \left[\frac{\sum t_i C_i}{\sum C_i} \right]^2 \quad [2]$$

where C_i = concentration of the salt exiting the reactor at time t_i , [mol m⁻³], t_i = time, [s], t_E^2 = dimensional mean exit age of molecules in the flow stream, [s²], and σ^2 = dimensional variance, [s²].

Equation [2] was fitted to the data to obtain the variance of the breakthrough curve. Knowing and using σ^2 the dispersion boundary conditions for an "open" flow system permits calculation of $\frac{D_i}{u_L l}$ from (10):

$$\sigma_\theta^2 = \frac{\sigma^2}{t^2} = 2 \left(\frac{D_i}{u_L l} \right) + 8 \left(\frac{D_i}{u_L l} \right)^2 \quad [3]$$

where t = mean residence time of molecules in the flow stream, [s] and σ_θ^2 = dimensionless variance, [-].

Development of Analytical Model for Ozone Mass Transfer

In order to obtain the mass transfer coefficient, $K_L a$, a description of the flow regime within the reactor was necessary. For simplicity, the flow pattern of the reactor was initially modeled as plug flow. To describe the gas flow in the reactor, as well as the axial concentration profile for the gas and liquid phase, the model domain as a first approximation was limited to the height of the diffuser, since that is the region of most active mass transfer. The mass balance, including ozone mass transfer, is given by Equation [1], for plug flow. The gas flow can be approximated by:

$$G = G_0 \frac{Z}{Z_0} \quad [4]$$

where G = volumetric gas flow rate into the aqueous phase of the reactor at Z , [m³s⁻¹], G_0 = volumetric gas flow rate to the diffuser, [m³s⁻¹], Z = coordinate along the axis of the reactor, [m], and Z_0 = height of the diffuser, [m].

Since the diffuser porosity and gas flow rate are assumed to be uniform along the length of the diffuser. $Z = 0$ at the bottom of the reactor, where water enters the reactor.

Based on the definition of the Henry's constant, $H = \frac{C_G}{C_{OL}}$, where C_G is the concentration of ozone in the gas phase [mol m⁻³]. Since it is necessary to know C_{OL} for the mass balance in Equation [1], C_G must be determined.

C_G was obtained by a mass balance at any height in the reactor between the gas and liquid phases given by

$$L(C_{OL} - C_0) = G(C_{G0} - C_G) \quad [5]$$

where L = volumetric liquid flow rate, [m³s⁻¹], C_{G0} = gaseous ozone concentration entering the reactor, [mol m⁻³], and C_0 = inlet aqueous phase concentration of ozone, [mol m⁻³].

The values of L , C_{G0} , and C_0 were constant throughout each experiment. All experiments were run with $C_{G0} \approx 80$ gm⁻³. We assume C_G is constant within the reactor. The gas phase concentration is well mixed at the entry of the reactor, and we assume that at these gas flow rates, there is no significant gas-phase concentration gradient inside the microporous tube.

$K_L a$ was correlated with both liquid and gas flow rates according to the following power-law expression (11):

$$K_L a = AL^\alpha G^\beta = AL^\alpha \left(\frac{G_0 Z}{Z_0} \right)^\beta \quad [6]$$

where A [s⁻¹], α [-], and β [-] are constant coefficients (Perry et al., 1997). Combining Equations [4] - [6] into Equation [1], the species balance equation becomes:

$$\frac{d^2 C_{OL}}{dZ^2} = \frac{1}{D_i} \left(u_L \left(\frac{dC_{OL}}{dZ} \right) + \left(\frac{AL^\alpha}{u_L} \right) \left(\frac{G_0 Z}{Z_0} \right)^\beta \left[\left(\frac{C_{G0} - \frac{LC_{OL}Z_0}{G_0 Z}}{H} - C_{OL} \right) \right] \right) \quad [7]$$

In order to obtain the constant coefficients and solve for $K_L a$ at varying flow rates, a nonlinear numerical code was applied. The Improved Euler Extrapolation (IEX) program, which integrates ordinary differential equations, was used for this purpose (Hanna and Sandall, 1995). Equation [7] was integrated up to Z_0 for a chosen value of AL^α . For a given experimental run, AL^α was adjusted until the calculated C_L at $Z = Z_0$ matched the measured values. This procedure was followed for each run. The values for the parameters A and α were obtained using a least squares fit from a log-log plot of AL^α versus L .

Mass Transfer Area Visualization

Photographic images of the gas bubbles were obtained along the length of the reactor with gas flow rate of 8.92×10^{-6} m³s⁻¹ and water flow rate of 1.67×10^{-5} m³s⁻¹. The photos were divided into seven sections along the height of the reactor, with each section containing a relatively uniform size of gas bubbles.

The lower part of the reactor contained gas bubbles with spherical shapes. The diameters of the visible bubbles ranged from 0.5 to 2 mm. The image from the lower region of the reactor was divided vertically into three sub-regions. In each sub-region, a 1-cm² area of the photograph was chosen to calculate the surface area of the spherical bubbles. Five areas were randomly selected.

The mean and standard deviation of the surface area was calculated based on the data from the selected cell. The overall surface area of each sub-region and of the whole image was then calculated based on the mean surface area. The surface area of the bubbles that were obscured from the camera by the diffuser was estimated by simply adding the same bubble surface area that had been estimated for the exposed part of the diffuser.

For the upper section of the reactor, where there was noticeable gas bubble coalescence, fewer but larger bubbles were observed, and the shapes were not spherical but elongated. Above the diffuser, the length of the bubbles ranged from 3 to 35 mm with diameters from 3 to 15 mm. In this region, all the bubbles in the images were first labeled, and then the surface area of each was estimated using a combination of cylinders capped with half spheres.

RESULTS

Experimental Measurement of Ozone Mass Transfer

Figure 2 presents results for experiments at $G_o = 1.67 \times 10^{-5} \text{ m}^3\text{s}^{-1}$ and different liquid flow rates ranging from 8.3×10^{-6} to $2.1 \times 10^{-5} \text{ m}^3\text{s}^{-1}$, indicating the rise in aqueous ozone concentration along the height of the reactor. Along the lower portion of the reactor, all of the experiments show mass transfer occurring linearly with Z . This is most likely observed because the total amount of ozone gas that enters the reactor also has a linear relationship with the height of the diffuser, as given in Equation [5]. Therefore, at the $Z = Z_o = 0.867 \text{ m}$, which is the top of the diffuser, all of the gas has entered into the aqueous phase via the diffuser. After this point in the reactor, the bubbles are seen to coalesce and not much more mass transfer is seen, with an aqueous ozone concentration profile nearly constant.

For the experiments using the higher gas flow rates, the aqueous ozone concentration is near saturation, especially at the lower liquid flow rates. The equilibrium aqueous ozone concentration is $\sim 21 \text{ gm}^{-3}$. In contrast, at low gas flow rates,

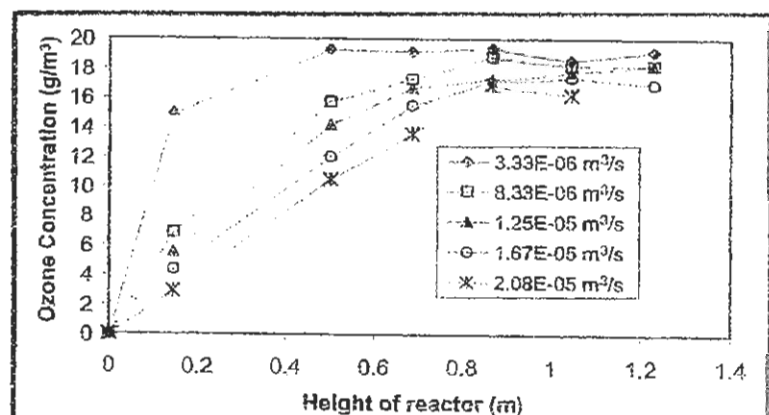


FIGURE 2. Aqueous ozone concentration along the length of reactor with a gas flow rate of $1.67 \times 10^{-5} \text{ m}^3\text{s}^{-1}$ and different water flow rates.

the aqueous ozone concentration was far from saturation. Most of the experiments indicated a very high transfer rate of ozone from the gas phase to liquid phase.

Residence Time Distribution (RTD)

Figure 3 shows a representative RTD experiment for a given water flow rate and varying gas flow rates. For all of these experiments, a higher gas or liquid flow rates produced a smaller D_L , indicating that the reactor approximates plug flow under these conditions. Values of D_L are listed in Table 1 for each corresponding flow rate. There is a linear relationship between D_L and L for each G , with correlation coefficient, r^2 [-], above 0.90. The equations at different gas flow rates are presented in Table 2. We can thus calculate the dispersion number at any liquid or gas flow rate within the range of our experiments.

Reactor Model Parameter Values

The mathematical model used in this study was confined to the height of the diffuser in the reactor. This was done since the concentration of ozone in the aqueous phase changes very little above the diffuser for almost all of the gas and water flow rates used in the model. Most of the mass transfer of ozone occurs within the length of the diffuser.

We first assumed that D_i would be negligible in Equation [7] and set it to zero. This simplified the initial

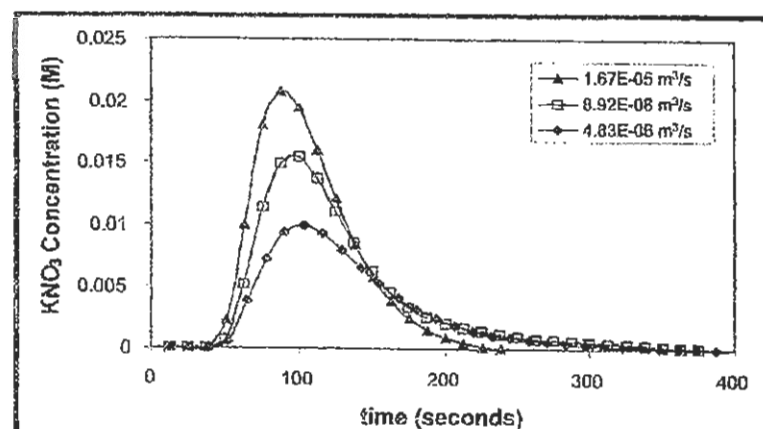


FIGURE 3. Residence time distribution for a water flow rate of $3.33 \times 10^{-6} \text{ m}^3\text{s}^{-1}$ and different gas flow rates.

TABLE 1. D_L at Different Gas and Liquid Flow Rates

Liquid flow rate (m^3/s)	Gas flow rate (m^3/s)		
	4.83×10^{-6}	8.92×10^{-6}	1.67×10^{-5}
3.33×10^{-6}	0.0937	0.1001	—
8.33×10^{-6}	0.0588	0.0547	0.0516
1.25×10^{-5}	0.0472	0.0387	0.0288
2.08×10^{-5}	0.0262	0.0194	0.0132

TABLE 2. Linear Correlation of D_L with L and G

Liquid flow rate (L) (m^3/s)	Gas flow rate (G) (m^3/s)	D_L correlation	r^2
$3.33 \times 10^{-6} - 2.08 \times 10^{-5}$	4.83×10^{-6}	$D_L = -0.0040 L + 0.103$	0.90
$3.33 \times 10^{-6} - 2.08 \times 10^{-5}$	8.92×10^{-6}	$D_L = -0.0040 L + 0.098$	0.92
$3.33 \times 10^{-6} - 2.08 \times 10^{-5}$	1.67×10^{-5}	$D_L = -0.0026 L + 0.066$	0.93

TABLE 3. Dependence of A and α on β

β	A (s/m^6)	α	r^2
0.40	6.330×10^8	1.5202	0.89
0.45	3.956×10^8	1.4323	0.85
0.50	2.297×10^9	1.5278	0.84
0.75	9.533×10^9	1.4001	0.77

integration of Equation [7], since most of the parameter values were known or measured except A , α and β . Four values of β were chosen, namely 0.40, 0.45, 0.50, 0.75; these values were chosen based on a literature value of 0.45 for β in a mixed reactor (Levenspiel, 1999). The corresponding A and α values at different β are presented in Table 3. $\beta = 0.40$ resulted in the best fit. Values of $K_L a$ for the reactor at varying gas and liquid flow rates are presented in Figure 4, with the values ranging from $0.0229 s^{-1}$ to $0.553 s^{-1}$. After obtaining D_i from the RTD experiments for all of the gas and liquid flow rates, we used Equation [7] with the experimental D_i to recalculate $K_L a$. The best correlation for $K_L a$ is:

$$K_L a = 3.96 \times 10^8 L^{1.53} G^{0.40} \quad [8]$$

with L and G in $m^3 s^{-1}$ and $K_L a$ in s^{-1} .

Although the correlation improved slightly by including D_i in Equation [7], the effect was almost negligible. This indicates that the dispersion in the reactor is small enough to be neglected in the model, in particular at higher liquid and gas flow rates.

Mass Transfer Area

Some examples of the bubble images are presented in Figures 5, 6, and 7. The area of the bubbles along the length of the reactor is presented in Figure 8, for $G = 8.92 \times 10^{-6} m^3 s^{-1}$ and $L = 1.67 \times 10^{-5} m^3 s^{-1}$. The total surface area of the bubbles in the reactor was $0.235 m^2$. At the end of the diffuser, the bubble area was $0.206 m^2$. The area of the bubbles was also examined using the same gas flow rate but with zero water flow rate, and the results showed that the total surface area of the bubbles was $\sim 22\%$ larger. The surface area of the bubbles were obtained in order to calculate a in $K_L a$, where a = surface area of the bubbles / volume in the reactor. The value of a was $624 m^{-1}$ for this reactor system under these flow conditions.

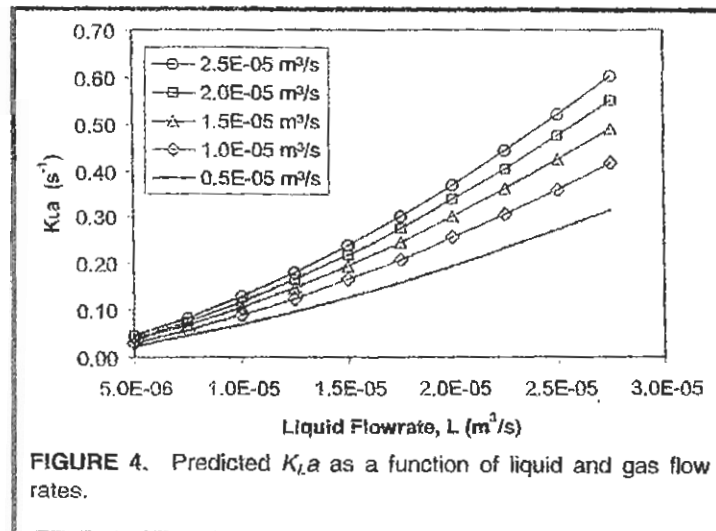


FIGURE 4. Predicted $K_L a$ as a function of liquid and gas flow rates.

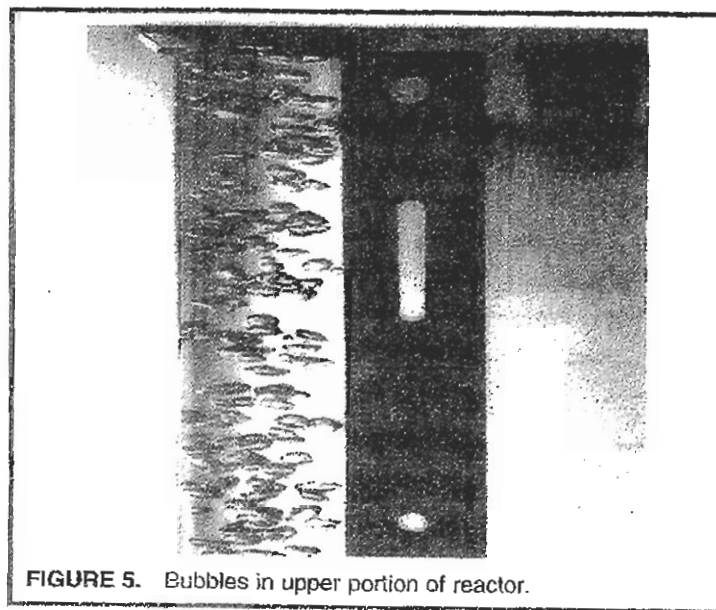


FIGURE 5. Bubbles in upper portion of reactor.

CONCLUSIONS

The experimental data of aqueous ozone concentrations along the length of the reactor indicated concentrations that were close to saturation for the higher flow rates, which would indicate a high mass transfer rate. However, to evaluate the performance of the reactor, the ozone mass transfer coefficient, $K_L a$, needed to be calculated and compared to other reactor systems. $K_L a$ values in the literature for bubble reactors with diffuser pore sizes 10

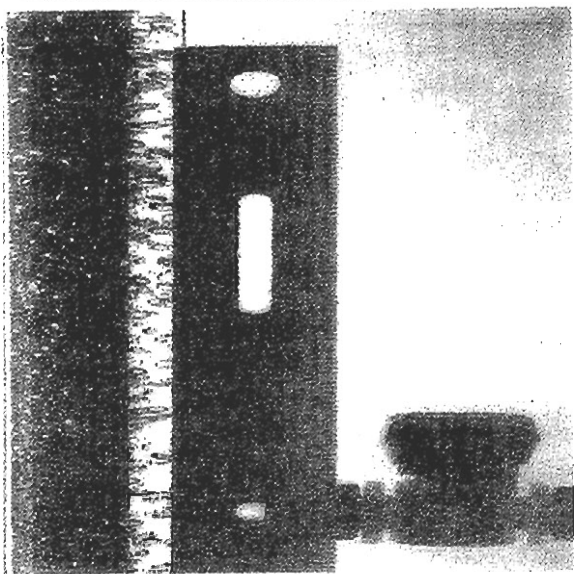


FIGURE 6. Bubbles in middle portion of reactor.

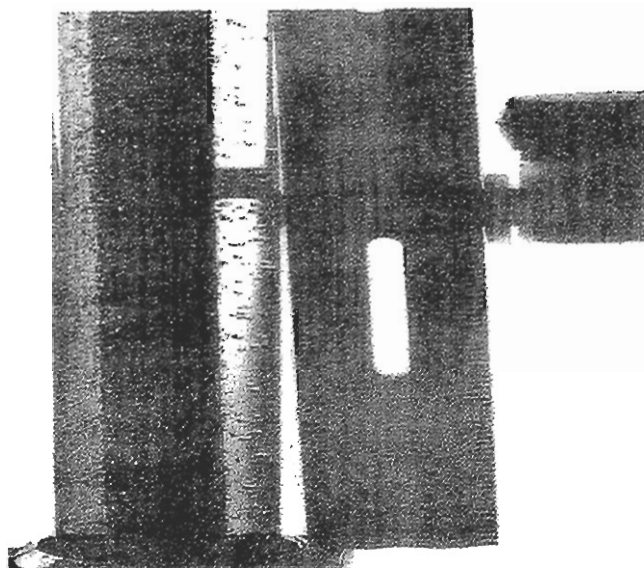


FIGURE 7. Bubbles in lower portion of reactor.

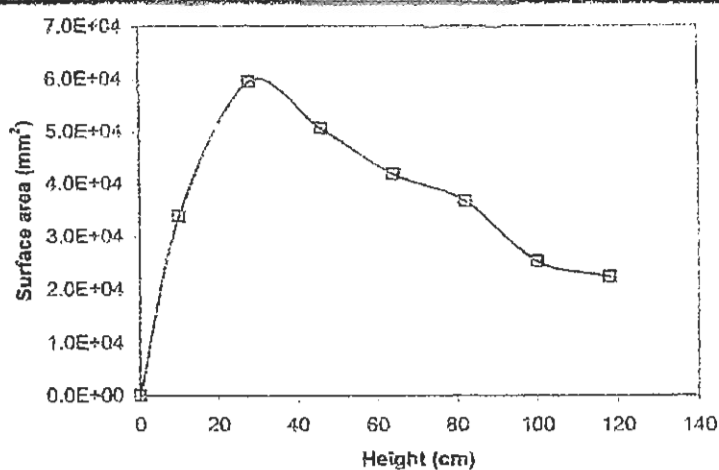


FIGURE 8. Bubble surface area along height of reactor, for $G = 8.92 \times 10^{-6} \text{ m}^3/\text{s}$ and $L = 1.67 \times 10^{-5} \text{ m}^3/\text{s}$.

to 100 times larger than the microporous diffuser used in this study range from 0.0083 up to 0.032 s^{-1} . The diffusers in these studies also do not extend throughout the length of the reactor. Comparing our results with these studies under similar temperature and pressure as reported in (Qiu et al., 2001, Roustan et al., 1996; Zhou and Smith, 2000), $K_L a = 0.023 \text{ s}^{-1}$ for the microporous reactor at $G = 4.83 \times 10^{-6} \text{ m}^3/\text{s}$ and $L = 1.67 \times 10^{-5} \text{ m}^3/\text{s}$.

When the liquid flow rate is increased, a very large increase in the $K_L a$ value can be obtained with our system. For example, when the liquid flow rate was increased from 3.33×10^{-6} to $2.08 \times 10^{-5} \text{ m}^3/\text{s}$ at a constant gas flow rate of $1.50 \times 10^{-5} \text{ m}^3/\text{s}$, the $K_L a$ value increases by ~ 14 times, from 0.0223 to 0.316 s^{-1} . K_L at this flow rate was calculated as $4.85 \times 10^{-4} \text{ m}^3/\text{s}$. This value was comparable to other literature values (Higbie, 1935; Hughmark, 1967; Roustan et al., 1981; Zhou and Smith, 2000). When K_L was extrapolated for an average bubble diameter in our reactor system ($\sim 1.3 \text{ mm}$), our K_L matched the literature value within 12%.

Most studies conclude that with conventional bubble diffusers, the gas flow rate is the most important factor affecting the ozone mass transfer coefficient. However, with a microporous diffuser that extends throughout the length of a tubular reactor, our studies indicate that for this reactor, the liquid flow rate plays a significant role on the rate of ozone mass transfer, since $\alpha > \beta$.

This may be due to the shearing effect of the liquid on the sub-micron gas bubbles as they are forced through the very small pores of the diffuser. Therefore, a higher liquid flow rate may result in a larger number of smaller bubbles in the stream, increasing the surface area for mass transfer to occur. The reactor is essentially plug flow at high G or L , which is a better configuration for an ozone reactor. This system achieves one of the highest ozone mass transfer rates observed in the literature.

ACKNOWLEDGMENTS

The authors wish to acknowledge funding from GRT, Inc. for most of this work, as well as the useful comments provided by Phil Grosso during the design of the reactor. We also would like to acknowledge the significant contributions of Vincent Martin and Dr. Sanya Sirivithayapakorn to the experimental work.

REFERENCES

1. Bader, H., and J. Hoigne, "Determination of Ozone in Water Using the Indigo Dye Method," *Ozone Sci. Eng.*, 4(4):169-176 (1982).
2. Boufaif, M., and M. Roustan, "Bubble Size and Mass Transfer Coefficients in Dual-Impeller Agitated Reactors," *Can. J. Chem. Eng.*, 76:390-397 (1998).
3. Hanna, O. T., and O. C. Sandall, *Computational Methods in Chemical Engineering* (Upper Saddle River, NJ: Prentice Hall, 1995).

4. Higbie, R., "Highbie: The Rate of Absorption of a Pure Gas into a Still Liquid," *Trans. Am. Inst. Chem. Engrs.* 31:365 (1935).
5. Hughmark, G. A., "Hughmark: Holdup in Gas-Liquid Flow," *Ind. Eng. Chem. Process. Des. Dev.* 6(2):218-220 (1967).
6. Le Sauze, N., A. Laplanche, N. Martin, and G. Matrin, "Modelling of Ozone Transfer in a Bubble Column," *Water Resources* 27(6):1071-1083 (1993).
7. Levenspiel, O., *Chemical Reaction Engineering, 3rd Ed.* (New York: John Wiley and Sons, Inc., 1999).
8. Mtarjemi, M., and G.J. Jameson, "Mass Transfer from Very Small Bubbles—The Optimum Bubble Size for Aeration," *Chem. Eng. Sci.* 33:1415-1423 (1978).
9. Ohkawa, A., Y. Kawai, D. Kusabiraki, N. Sakai, and K. Endoh, "Bubble Size, Interfacial Area, and Volumetric Liquid Phase Mass Transfer Coefficient in Downflow Bubble Columns with Gas Entrainment by a Liquid Jet," *J. Chem. Eng. Japan* 20(1):99-101 (1983).
10. Qiu, Y., C. Kuo, and M.E. Appi, "Performance and Simulation of Ozone Absorption and Reactions in a Stirred Tank Reactor," *Environ. Sci. Tech.*, 35:209-215 (2001).
11. Perry, R. H., D.W. Green, and J.O. Maloney, *Chemical Engineers' Handbook, 7th Ed.* (New York: McGraw-Hill Professional, 1997).
12. Rinker E. B. S. S. Ashour, M. C. Johnson, G. J. Kott, R. G. Rinker, and O. C. Sandall, "Kinetics of the Aqueous Phase Reaction between Ozone and 2,4,6-trichlorophenol," *AIChE J.* 45(8):1802-1807 (1999).
13. Roustan, M. J. H. Mallevialle, Roques, and J. P. Jones, "Mass Transfer of Ozone to Water: A Fundamental Study," *Ozone Sci. Eng.* 2:337-344 (1981).
14. Roustan, M., R.Y. Want, and D. Wolbert, "Modeling Hydrodynamics and Mass Transfer Parameters In a Continuous Ozone Bubble Column", *Ozone Sci. Eng.* 18:99-115 (1996).
15. Zhou, H., and D. W. Smith, "Ozone Mass Transfer in Water and Wastewater Treatment," *Water Res.*, 34(3):909-921 (2000).